GENERALIZED GREEN'S FUNCTIONS AND THE EFFECTIVE DOMAIN OF INFLUENCE

DONALD ESTEP [*], MICHAEL HOLST [†], AND MATS LARSON [‡]

Abstract. One well-known approach to *a posteriori* analysis of finite element solutions of elliptic problems estimates the error in a quantity of interest in terms of residuals and a generalized Green's function. The generalized Green's function solves the adjoint problem with data related to a quantity of interest and measures the effects of stability, including any decay of influence characteristic of elliptic problems. We show that consideration of the generalized Green's function can be used to improve the efficiency of the solution process when the goal is to compute multiple quantities of interest and/or to compute quantities of interest that involve globally-supported information such as average values and norms. In the latter case, we introduce a solution decomposition in which we solve a set of problems involving localized information, and then recover the desired information by combining the local solutions. By treating each computation of a quantity of interest independently, the maximum number of elements required to achieve the desired accuracy can be decreased significantly.

Key words. *a posteriori* error estimates, adaptive error control, adaptive mesh refinement, adjoint problem, coarse-grained parallelization, decay of influence, domain decomposition, effective domain of influence, dual problem, efficient discretization, elliptic problem, error estimates, finite element method, generalized Green's function, localization, residual error, solution decomposition, stability, variational analysis

AMS subject classifications. 65N15, 65N30, 65N50

1. Introduction. A characteristic property of elliptic partial differential equations is a *global* domain of influence. That is, a local perturbation of data near one point affects the solution throughout the domain of the problem. Indeed, in the extreme case of an analytic harmonic function, prescribing the values of a solution on any small sub-domain or even on a piece of curve suffices to define its values throughout the domain. Of course, this property has profound consequences for the numerical solution of elliptic equations.

Yet when taken out of context, this property can give a misleading impression. In particular, elliptic problems often have the property that the strength of the effect of a localized perturbation on a solution decays significantly with the distance from the support of the perturbation, at least in some directions. It turns out that this property also has profound consequences for the numerical solution of elliptic problems, which we explore in this paper.

One way to see the decay of influence in an elliptic problem is to consider the properties of Green's functions. Green's functions play the role of fundamental solutions for boundary value problems on finite domains. To simplify the presentation,

---

we consider the Dirichlet problem for a second order linear elliptic operator $L(D, x)$,

$$\begin{cases} L(D, x)u(x) = f(x), & x \in \Omega, \\ u(x) = 0, & x \in \partial\Omega, \end{cases} \tag{1.1}$$

where Ω is a smooth or polygonal domain in $\mathbb{R}^d$, $d = 2$ or 3 and the coefficients of L and the data f are suitably smooth. Suppose that $y \in \Omega$ and let δ_y denote the delta distribution at y. The Green's function $G(y, x)$ for (1.1) satisfies the *adjoint boundary value problem*,

$$\begin{cases} L^*(D, x)G(y, x) = \delta_y(x), & x \in \Omega, \\ G(y, x) = 0, & x \in \partial\Omega, \end{cases} \tag{1.2}$$

where the *adjoint operator* $L^*(D, x)$ satisfies

$$(L(D, \cdot)u(\cdot), v(\cdot)) = (u(\cdot), L^*(D, \cdot)v(\cdot)) \tag{1.3}$$

for all smooth functions u, v with compact support in $\overline{\Omega} = \Omega \cup \partial\Omega$, with $(\ ,\ )$ denoting the L^2 inner product on Ω. For example, if

$$L(D, x)u = -\nabla \cdot a(x)\nabla u + b(x) \cdot \nabla u + c(x)u(x), \tag{1.4}$$

where $u : \mathbb{R}^d \to \mathbb{R}$, a is a $d \times d$ matrix function of x, b is a d-vector function of x, and c is a function of x, then

$$L^*(D, x)v = -\nabla \cdot a(x)^\top \nabla v - \operatorname{div}(b(x)v) + c(x)v(x),$$

where $a^\top$ is the transpose of a.

Because of the boundary conditions in (1.1) and (1.2), for $y \in \Omega$,

$$\big(f(\cdot), G(y, \cdot)\big) = \big(L(D, \cdot)u(\cdot), G(y, \cdot)\big) = \big(u(\cdot), L^*(D, \cdot)G(y, \cdot)\big) = \big(u, \delta_y\big) = u(y), \tag{1.5}$$

when the integrals are defined. In other words, the solution of (1.1) is given by

$$u(y) = \int_\Omega G(y, x)f(x)\, dx, \quad y \in \Omega, \tag{1.6}$$

when the integral on the right is defined. In the case of a boundary value problem with general boundary conditions, the integration by parts (1.3) that defines the adjoint yields generally nonzero boundary integrals over the boundary $\partial\Omega$. The Green's function is a solution of the adjoint differential equation chosen to yield the analog of the representation (1.6) and to simplify any boundary integrals, see [20].

In this paper, we are concerned with the effects of perturbations on the data. If the data f is perturbed by a smooth function δf, the perturbation in the value of the solution $\delta u(y)$ is given by

$$\delta u(y) = \int_\Omega G(y, x)\delta f(x)\, dx, \quad y \in \Omega. \tag{1.7}$$

Of course, we interpret (1.2) in a weak sense. Standard elliptic theory yields the existence of the solution G of (1.2), and in a very few special cases, we can even find a

formula for the Green's function. For example, the Green's function for the Dirichlet problem for the Laplacian $L = -\Delta$ on the ball Ω of radius r centered at the origin is

$$G(y, x) = \frac{1}{4\pi} \times \begin{cases} |y - x|^{-1} - r|y|^{-1}\left|\frac{r^2 y}{|y|^2} - x\right|^{-1}, & y \neq 0, \\ |x|^{-1} - r^{-1}, & y = 0, \end{cases}$$

where $|x|$ denotes the Euclidean norm of x. If δf has compact support $\mathrm{supp}(\delta f) \subset \Omega$, then a simple geometrical argument shows that

$$|y - x| \leq \left|\frac{r^2 y}{|y|^2} - x\right|, \quad x \in \mathrm{supp}(\delta f),\ y \in \Omega \setminus \mathrm{supp}(\delta f).$$

We conclude that

$$|\delta u(y)| \leq \frac{\max |\delta f| \ \times \ \text{volume of } \ \mathrm{supp}(\delta f) \times \left(1 + \frac{r}{|y|}\right)}{4\pi \times \text{the distance from } y \text{ to } \mathrm{supp}(\delta f)},$$

and the effects of a local perturbation in the data decays with the distance to the support of the perturbation.

In this paper, we explore the consequences of the decay of influence for the numerical solution of elliptic problems. Our chief tool is an *a posteriori* error analysis that involves an generalization of the notion of a Green's function, which determines the propagation and decay of influence of discretization error in a quantity of interest. Using the generalized Green's function, we define the notion of an *effective* domain of influence. In order to achieve accuracy in the desired quantity, a mesh must be sufficiently refined inside the effective domain of influence, while outside the effective domain, the mesh may be relatively coarse. This turns out to be useful in terms of computing efficiently.

We begin in Sec. 3 with a simple example of a finite element discretization of Poisson's equation in a disk. Using an *a posteriori* analysis together with formula for the Green's function, we show that the error in the energy norm in a small region is affected relatively little by discretization errors committed away from the region. This means we can compute a numerical solution with accurate values in a small region using a mesh that is fine near the region and coarse away from the region. The effective domain of influence is the region requiring the fine mesh.

In Sec. 4, we consider a general linear elliptic problem as well as the generalized Green's function corresponding to a particular quantity of interest. We explain how the generalized Green's function can be used in adaptive error control to produce an efficiently refined mesh. Since, it is usually impossible to find an explicit formula for the generalized Green's function, we discuss its numerical approximation as well.

In Sec. 5, we explain how the problem of computing multiple quantities of interest simultaneously arises naturally in practice and also when the data for the generalized Green's function does not have spatially localized support. In that case, we introduce a partition of unity to localize the data for the generalized Green's function and, in effect, to decompose the solution process. In Sec. 6, we then explain how explicit knowledge of the effective domains of influence corresponding to multiple quantities of interest can be used to compute the solution efficiently.

The solution decomposition introduced in Sec. 5 raises the two issues of identifying the effective domain of influence in terms of a given mesh and recognizing whether two effective domains of influence are more-or-less distinct or not. We address these issues in Sec. 7.

Finally, we present several computational examples illustrating these ideas in Sec. 8 and conclude in Sec. 9.

Acknowledgements. The authors gratefully thank James Stewart, Sandia National Laboratories and Simon Tavener, Colorado State University for their comments.

2. Finite element discretization. We consider the second order linear elliptic boundary value problem (1.1) with L defined by (1.4). We assume that $\Omega \subset \mathbb{R}^d$, $d = 2, 3$, is a smooth or polygonal domain; $a = (a_{ij})$, where $a_{i,j}$ are continuous in $\overline{\Omega}$ for $1 \leq i, j \leq n$ and there is a $a_0 > 0$ such that $v^\top a v \geq a_0$ for all $v \in \mathbb{R}^d \setminus \{0\}$ and $x \in \Omega$; $b = (b_i)$ where b_i is continuous in $\overline{\Omega}$; and finally c and f are continuous in $\overline{\Omega}$.

For a region Ω in $\mathbb{R}^d$, $d = 2, 3$, we use $L^2(\Omega)$ to denote the space of square integrable functions with inner product, $(u, v) = (u, v)_\Omega = \int_\Omega u \cdot v \, dx$, and corresponding norm $\|u\| = \|u\|_\Omega = (u, u)^{1/2}$, with the obvious interpretation for scalar or vector valued functions. We use $H^p(\Omega)$ to denote the space of functions that are in $L^2(\Omega)$ and whose derivatives up to order p are in $L^2(\Omega)$, with the usual norm. We use $H_0^1(\Omega)$ to denote the subspace of $H^1(\Omega)$ consisting of functions that are zero on the boundary $\partial\Omega$ of Ω. We also use the seminorm, $|v|_{1,\Omega} = \|\nabla v\|_\Omega$.

We discretize (1.1) by applying a finite element method to the associated variational formulation:

Find $u \in H_0^1(\Omega)$ such that

$$A(u, v) = (a\nabla u, \nabla v) + (b \cdot \nabla u, v) + (cu, v) = (f, v) \text{ for all } v \in H_0^1(\Omega). \quad (2.1)$$

To construct a finite element discretization, we form a piecewise polygonal approximation of $\partial\Omega$ whose nodes lie on $\partial\Omega$ and which is contained inside Ω. This forms the boundary of a convex polygonal domain Ω_h. We let $\mathcal{T}_h$ denote a simplex triangulation of Ω_h that is locally quasi-uniform. We let h_K denote the length of the longest edge of $K \in \mathcal{T}_h$ and define the piecewise constant mesh function h by $h(x) = h_K$ for $x \in K$. We also use h to denote $\max_K h_K$. We choose a finite element solution from the space V_h of functions that are continuous on Ω, piecewise linear on Ω_h with respect to $\mathcal{T}_h$, zero on the boundary $\partial\Omega_h$, and finally extended to be zero in the region $\Omega \setminus \Omega_h$. With this construction, we have $V_h \subset H_0^1(\Omega)$, and for smooth functions, the error of interpolation into V_h is $\mathbf{O}(h^2)$ in $\| \ \|$, but not better (see [19]). The finite element method is:

$$\text{Compute } U \in V_h \text{ such that } A(U, v) = (f, v) \text{ for all } v \in V_h. \quad (2.2)$$

By standard results, we know that U exists and converges to u as $h \to 0$.

3. The Green's function and the error of a finite element solution of Poisson's equation in a disk. In this section, we analyze an example for which there is a formula for the Green's function. We let Ω denote the disk of radius r centered at the origin in $\mathbb{R}^2$, and consider the Dirichlet problem (1.1) with $L = -\Delta$. Suppose that ω is a small region contained in Ω located well away from $\partial\Omega$ and that we wish to estimate the error $e = u - U$ in the energy norm $\|e\|_{1,\omega}$ in ω. We use the *a posteriori* error analysis introduced in [9] closely, varying only the data for the adjoint problem and the way the bounds on the *a posteriori* estimate are written. With $H^{-1}(\omega)$ denoting the dual space to $H^1(\omega)$ and $\| \ \|_{-1,\omega}$ the associated norm, we can evaluate the norm variationally as

$$\|e\|_{1,\omega} = \sup_{\substack{\psi \in H^{-1}(\omega) \\ \|\psi\|_{-1,\omega}=1}} (e, \psi). \quad (3.1)$$

The supremum is achieved for some $\psi \in H^{-1}(\omega)$. We extend this ψ to $H^{-1}(\Omega)$ by setting it to zero in $\Omega \setminus \omega$. Let ϕ solve the adjoint, or dual, problem:

Find $\phi \in H_0^1(\Omega)$ such that $A(v, \phi) = (v, \psi)$ for all $v \in H_0^1(\Omega)$.

We obtain

$$\|e\|_{1,\omega} = (e, \psi) = A(e, \phi) = \int_\Omega \nabla e \cdot \nabla \phi \, dx = \int_\Omega f\phi \, dx - \int_\Omega \nabla U \cdot \nabla \phi \, dx.$$

Using the Galerkin orthogonality (2.2), we obtain the *error representation formula*,

$$\|e\|_{1,\omega} = \int_\Omega f(\phi - \pi_h \phi) \, dx - \int_\Omega \nabla U \cdot \nabla (\phi - \pi_h \phi) \, dx, \tag{3.2}$$

where $\pi_h \phi$ is an approximation of ϕ in V_h. The representation (3.2) is the finite element-energy norm analog of the Green's function representation (1.7) of the effect of perturbing the data.

From (3.2), we obtain a standard *a posteriori* error bound in terms of the residual $\mathcal{R}_K$ and corresponding adjoint weights $\mathcal{W}_K$ similar to the result in [9].

THEOREM 3.1. *The energy norm error of the finite element approximation (2.2) on ω is bounded by*

$$\|e\|_{1,\omega} \le \sum_{K \in \mathcal{T}_h} \mathcal{R}_K \cdot \mathcal{W}_K = \sum_{K \in \mathcal{T}_h} \left(\begin{array}{c} \|\Delta U + f\|_K \\ \|h^{-1/2}[\nabla U]\|_{\partial K}/2 \end{array} \right) \cdot \left(\begin{array}{c} \|\phi - \pi_h \phi\|_K \\ \|h^{1/2}(\phi - \pi_h \phi)\|_{\partial K} \end{array} \right),$$

where $n_{\partial K}$ denotes the outward normal to ∂K and $[U]$ denotes the "jump" in ∇U across an edge of K in the direction of the normal $n_{\partial K}$. The residual is bounded by a mesh-independent constant C in the sense that

$$\mathcal{R}_K \le C|K|^{1/2}, \tag{3.3}$$

*where $|K|$ denote the area of $K \in \mathcal{T}_h$.*

The proof is given in the Appendix.

Clearly, the convergence of the Galerkin approximation is strongly influenced by the dual weights $\phi - \pi_h \phi$, i.e. by the approximation properties of V_h and the smoothness of ϕ. This reflects the importance of the cancellation of errors inherent to the Galerkin method. If we let $G(x, y)$ denote the Green's function for the Laplacian on Ω, then

$$\phi(x) = \int_\Omega G(x, y)\psi(y) \, dy = \int_\omega G(x, y)\psi(y) \, dy.$$

There are two cases to consider. For $y \in \omega$, $G(x, y)$ is a smooth function of x for $x \in \Omega \setminus \omega$, and therefore so is ϕ. We assume that $\delta > 0$ is small enough that $\omega_\delta = \{x \in \Omega : \text{dist}\,(x, \omega) \le \delta\}$ is contained in Ω, but large enough that for $K \subset \Omega \setminus \omega_\delta$, the union $\mathcal{N}(K)$ of K and the elements bordering K does not intersect ω, see Fig. 3.1. For $K \subset \Omega \setminus \omega_\delta$, we let π_h be the Lagrange nodal interpolant with respect to $\mathcal{T}_h$, so that

$$\|\phi - \pi_h \phi\|_K \le C \sum_{|\alpha|=2} \|h^2 D^\alpha \phi\|_K.$$
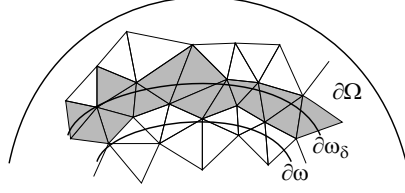
FIG. 3.1. *The choice of ω_δ.*

On the other hand, ϕ is only in $H^1(\omega)$ in general. For $K \cap \omega_\delta \neq \emptyset$, we let π_h be the Scott-Zhang interpolant ([5]), for which

$$\|\phi - \pi_h\phi\|_K \leq C|h\phi|_{1,\mathcal{N}(K)},$$

for a mesh-independent constant C.

The second component of $\mathcal{W}_K$ is bounded similarly after using a trace theorem,

$$\|h^{1/2}(\phi - \pi_h\phi)\|_{\partial K} \leq \|\phi - \pi_h\phi\|_{\mathcal{N}(K)}^{1/2}\|h(\phi - \pi_h\phi)\|_{1,\mathcal{N}(K)}^{1/2},$$

and the local quasi-uniformity of the mesh. We conclude,

THEOREM 3.2. *For any $\delta > 0$ small enough that $\omega_\delta \subset \Omega$ but large enough that $\mathcal{N}(K) \cap \omega = \emptyset$ for $K \subset \Omega \setminus \omega_\delta$, there is a constant C such that*

$$\|e\|_{1,\omega} \leq \sum_{K \subset \Omega \setminus \omega_\delta} \sum_{|\alpha|=2} C\|h^2 D^\alpha\phi\|_K|K|^{1/2} + \sum_{K \cap \omega_\delta \neq \emptyset} C|h\phi|_{1,\mathcal{N}(K)}|K|^{1/2}. \qquad (3.4)$$

To understand the implications of (3.4) for mesh selection in an adaptive setting, we further estimate the quantities on the right in (3.4). To handle the first sum, we estimate the derivatives using the Green's function as

$$\|D_x^\alpha\phi\|_K^2 = \int_K \left(\int_\omega D_x^\alpha G(x,y)\psi(y)\,dy\right)^2 dx \leq \int_K \|D_x^\alpha G(x,\cdot)\|_{1,\omega}^2\|\psi\|_{-1,\omega}^2\,dx$$

$$= \sum_{|\beta|=1}\int_K\int_\omega |D_x^\alpha D_y^\beta G(x,y)|^2\,dydx + \int_K\int_\omega |D_x^\alpha G(x,y)|^2\,dydx.$$

The Green's function for the Dirichlet problem for the Laplacian on the disk of radius r is given by

$$G(y,x) = \frac{1}{2\pi} \times \begin{cases} \ln\left(\frac{|y|\left|\frac{r^2 y}{|y|^2}-x\right|}{r|y-x|}\right), & y \neq 0, \\ \ln\left(\frac{r}{|x|}\right), & y = 0, \end{cases} \qquad (3.5)$$

so there is a constant C such that

$$|D_x^\alpha D_y^\beta G(x,y)| \leq \frac{C}{|x-y|^2}, \quad x \neq y \in \Omega, \ |\alpha| = 2, \ |\beta| \leq 1.$$

We conclude there is a constant C independent of the mesh such that for $K \subset \Omega \setminus \omega_\delta$,

$$\|\phi - \pi_h\phi\|_K \leq \frac{Ch_K^2}{\text{dist}\,(K,\omega)^2}|K|^{1/2}.$$

To handle the second sum on the right of (3.4), we use the basic stability estimate,

$$\|\phi\|_{1,\Omega} \leq \|\psi\|_{-1,\Omega} = \|\psi\|_{-1,\omega} = 1.$$

If we assume a uniform (small) size $h_K = \underline{h}$ for elements such that $K \cap \omega_\delta \neq \emptyset$, we obtain

$$\sum_{K \cap \omega_\delta \neq \emptyset} C h_K |\phi|_{1,\mathcal{N}(K)} \leq C\underline{h}\|\phi\|_{1,\Omega} = C\underline{h} = \frac{C}{|\omega_\delta|} \sum_{K \cap \omega_\delta \neq \emptyset} \underline{h}|K|.$$

We conclude

THEOREM 3.3. *For any $\delta > 0$ small enough that $\omega_\delta \subset \Omega$ but large enough that $\mathcal{N}(K) \cap \omega = \emptyset$ for $K \subset \Omega \setminus \omega_\delta$, there is a constant C such that*

$$\|e\|_{1,\omega} \leq \sum_{K \subset \Omega \setminus \omega_\delta} \frac{C h_K^2}{\operatorname{dist}(K,\omega)^2}|K| + \sum_{K \cap \omega_\delta \neq \emptyset} C\underline{h}|K|. \tag{3.6}$$

In common approaches to adaptive error control, a "Principle of Equidistribution" shows that the element contributions to the error are approximately equal in a nearly optimal mesh. In (3.6), the element indicators are $C h_K^2/\operatorname{dist}(K,\omega)^2$ respectively $C\underline{h}$, and in an optimal mesh,

$$\frac{h_K^2}{\operatorname{dist}(K,\omega)^2} \approx \underline{h} \quad \text{or} \quad h_K \approx \underline{h}^{1/2} \times \operatorname{dist}(K,\omega), \quad K \subset \Omega \setminus \omega_\delta.$$

The decay of influence inherent to the Laplacian on the disk means that away from the region ω where we estimate the norm, we can choose elements asymptotically larger than the element size used in ω_δ. Moreover, the elements can increase in size as the distance to ω_δ increases. In this problem, we call ω_δ the *effective domain of influence* for the error in the energy norm in ω. The effective domain of influence is characterized by the requirement that the mesh size needed for accurate computation is small in the effective domain relative to the size required in its complement.

4. An a posteriori error analysis using the generalized Green's function. In this section, we explain how the *a posteriori* error analysis presented in Sec. 3 can be extended to more general situations. Again, the analysis follows the ideas introduced in [9] closely, with the main difference being the choice of data for the adjoint problem.

Classical analysis of finite element methods tends to focus on estimating the error in global norms, such as $\| \quad \|_{L^2(\Omega)}$ or the energy norm. In practice, however, this may not be meaningful. Often, the practical goal for solving a differential equation is to compute specific information from the solution. In that situation, the concern is the error in the desired information, which may not have much to do with the error in some global norm.

In contrast, the goal of the *a posteriori* error analysis conducted below is to estimate the error in a quantity of interest that can be represented as (u, ψ), where ψ is some distribution in a suitable Sobolev space. Some useful choices of ψ include:
- $\psi = \chi_\omega/|\omega|$ gives the error in the average value over $\omega \subset \Omega$, where χ_ω is the characteristic function of ω.
- $\psi = \delta_x$ gives the error at a point x, $\psi = \delta_c$ gives the error in the average over a curve c in $\mathbb{R}^d$, $d = 2, 3$, and $\psi = \delta_s$ gives the error in the average over a plane surface s in $\mathbb{R}^3$. We can obtain errors in derivatives using dipoles in the same way.

- $\psi = \chi_\omega e / \|e\|_\omega$ gives the error in the $L^2(\omega)$ norm, $\|e\|_\omega$. In practice, good approximations can be obtained with Richardson extrapolation using finite element solutions with different accuracy.
- $\psi = \mathcal{R}$ gives the error in the energy norm when $b \equiv c \equiv 0$ and $\mathcal{R}$ is the residual defined weakly by $(\mathcal{R}, v) = (a\nabla U, \nabla v) - (f, v)$ for all $v \in H_0^1(\Omega)$.

Note that only some of these data ψ have spatially local support.

The *a posteriori* analysis that we employ suggests an extension of the classic concept of a Green's function, which is defined traditionally as the solution of the adjoint problem posed with data δ_y corresponding to the value $u(y)$. The natural extension corresponds to the data ψ that gives the desired information of the solution via (u, ψ). We define the *generalized Green's function* ϕ as the solution of the weak *adjoint problem*,

Find $\phi \in H_0^1(\Omega)$ such that
$$A^*(v, \phi) = (\nabla v, a\nabla \phi) - (v, \operatorname{div}(b\phi)) + (v, c\phi) = (v, \psi) \text{ for all } v \in H_0^1(\Omega), \quad (4.1)$$

corresponding to the adjoint problem $L^*(D, x)\phi = \psi$. Arguing as in Sec. 3,

$$
\begin{aligned}
(e, \psi) &= (\nabla e, a\nabla \phi) - (e, \operatorname{div}(b\phi)) + (e, c\phi) = (a\nabla e, \nabla \phi) + (b \cdot \nabla e, \phi) + (ce, \phi) \\
&= (f, \phi) - (a\nabla U, \nabla \phi) - (b \cdot \nabla U, \phi) - (cU, \phi).
\end{aligned}
$$

Letting $\pi_h \phi$ denote an approximation of ϕ in V_h, using Galerkin orthogonality, we conclude

THEOREM 4.1. *The error of the finite element solution (2.2) satisfies the* error representation,

$$(e, \psi) = (f, \phi - \pi_h \phi) - (a\nabla U, \nabla(\phi - \pi_h \phi)) - (b \cdot \nabla U, \phi - \pi_h \phi) - (cU, \phi - \pi_h \phi), \quad (4.2)$$

where the generalized Green's function ϕ satisfies the adjoint problem (4.1) corresponding to data ψ.

To obtain accurate error estimates, we use (4.2) directly by approximating ϕ using a finite element method. Since $\phi - \pi_h \phi \sim \sum_{|\alpha|=2} D^\alpha \phi$ where ϕ is smooth, we use a high order finite element method. For example, good results are obtained using the space V_h^2 of continuous, piecewise quadratic functions with respect to $\mathcal{T}_h$. The approximate generalized Green's function is

Compute $\Phi \in V_h^2$ such that
$$A^*(v, \Phi) = (\nabla v, a\nabla \Phi) - (v, \operatorname{div}(b\Phi)) + (v, c\Phi) = (v, \psi) \text{ for all } v \in V_h^2. \quad (4.3)$$

The corresponding *approximate error representation* is

$$(e, \psi) \approx (f, \Phi - \pi_h \Phi) - (a\nabla U, \nabla(\Phi - \pi_h \Phi)) - (b \cdot \nabla U, \Phi - \pi_h \Phi) - (cU, \Phi - \pi_h \Phi). \quad (4.4)$$

The use of the adjoint problem to obtain information about stability in *a posteriori* error analysis was introduced in [9]. The goal in that paper was to obtain reasonably accurate *a priori* bounds on the adjoint weights, and the paper dealt with the Poisson equation and the linear heat equation, for which this is possible. The idea of using a numerical approximation of the generalized Green's function to compute very accurate *a posteriori* estimates was introduced experimentally in [6] and developed in the context of nonlinear ordinary differential equations in [10] and nonlinear

partial differential equations in [13]. Since these early contributions, there has been substantial contributions and applications, see [7, 14, 4, 15, 2].

For the purpose of adaptive error control, we rewrite (4.4) as a sum of element contributions,

$$(e, \psi) \approx \sum_{K \in \mathcal{T}_h} \int_K \left((f - b \cdot \nabla U - cU)(\Phi - \pi_h \Phi) - a\nabla U \cdot \nabla(\Phi - \pi_h \Phi) \right) dx. \quad (4.5)$$

As in Sec. 3, we define the notion of an effective domain of influence through consideration of adaptive meshing. An ideal goal of adaptive error control is to find a mesh with a relatively small number of elements such that for a given tolerance TOL and data ψ, $|(e, \psi)| \le$ TOL . We use (4.5) to replace this with a practical *mesh acceptance criterion*:

$$\left| \sum_{K \in \mathcal{T}_h} \int_K \left((f - b \cdot \nabla U - cU)(\Phi - \pi_h \Phi) - a\nabla U \cdot \nabla(\Phi - \pi_h \Phi) \right) dx \right| \le \text{TOL}. \quad (4.6)$$

The standard variational "Principle of Equidistribution" argument requires an estimate consisting of an element-wise sum of positive quantities. Thus, if (4.6) is **not** satisfied, then the mesh is refined in order to achieve the more conservative condition,

$$\sum_{K \in \mathcal{T}_h} \int_K \left| (f - b \cdot \nabla U - cU)(\Phi - \pi_h \Phi) - a\nabla U \cdot \nabla(\Phi - \pi_h \Phi) \right| dx \le \text{TOL}. \quad (4.7)$$

Then, the element indicators on a nearly optimal mesh are roughly equal across the elements. Depending on the argument, we may use

$$\max_K \left| (f - b \cdot \nabla U - cU)(\Phi - \pi_h \Phi) - a\nabla U \cdot \nabla(\Phi - \pi_h \Phi) \right| \lesssim \frac{\text{TOL}}{|\Omega|}, \quad (4.8)$$

or

$$\int_K \left| (f - b \cdot \nabla U - cU)(\Phi - \pi_h \Phi) - a\nabla U \cdot \nabla(\Phi - \pi_h \Phi) \right| dx \lesssim \frac{\text{TOL}}{M}, \quad (4.9)$$

as *element acceptance criteria*, where M is the number of elements in $\mathcal{T}_h$. Computing a mesh using these criteria is usually performed by a "compute-estimate-mark-refine" adaptive strategy that begins with a coarse mesh and then refines those elements on which (4.8) respectively (4.9) fail if (4.6) is violated.

An *effective domain of influence* corresponding to the data ψ is the region ω_ψ in which the corresponding elements **must** be significantly smaller in size than the elements used in the complement $\Omega \setminus \omega_\psi$ in order to satisfy (4.6). Equivalently, if $\mathcal{T}_h$ comprises uniformly sized elements, then the effective domain of influence comprises those elements on which the element indicators (4.8), alternatively (4.9), are substantially larger than those in the complement.

5. A decomposition of the solution. It is often the case that the goal of solving a differential equation is to compute several pieces of information. For example, we might wish to compute values of the solution at a number of points and internal boundaries. In this section, we explain how the problem of computing multiple quantities of interest also arises naturally when the data ψ for the adjoint problem does not have spatially localized support, such as an average or norm over the domain Ω.

In general, we cannot expect a significant localizing effect from the decay of influence when the support of the data for the adjoint problem is not spatially localized. Certainly, if the data ψ has the property that the corresponding adjoint weight $\phi - \pi_h \phi$ has a more-or-less uniform size throughout Ω, then the degree of non-uniformity in an adapted mesh depends largely on the spatial variation of the residual.

However, we can use a partition of unity to "localize" a problem in which supp (ψ) does not have local support. We let $\{\Omega_i\}_{i=1}^N$ be a finite open cover of Ω. A *Lipschitz partition of unity* subordinate to $\{\Omega_i\}$ is a collection of functions $\{p_i\}_{i=1}^N$ with the properties

$$\text{supp}\,(p_i) \subset \overline{\Omega}_i, \quad 1 \le i \le N, \quad \sum_{i=1}^N p_i(x) = 1, \quad x \in \Omega, \tag{5.1}$$

$$p_i \text{ is continuous on } \Omega \text{ and differentiable on } \Omega_i, \quad 1 \le i \le N, \tag{5.2}$$

$$\|p_i\|_{L^\infty(\Omega)} \le C \text{ and } \|\nabla p_i\|_{L^\infty(\Omega_i)} \le C/\text{diam}\,(\Omega_i), \quad 1 \le i \le N, \tag{5.3}$$

where C is a constant and diam (Ω_i) is the diameter of Ω_i. Several partitions of unity satisfying (5.1)-(5.3) exist, see e.g. [16].

We use a partition of unity $\{p_i\}$ to write $\psi \equiv \sum_{i=1}^N \psi p_i$ and consider the problem of estimating the error in the *localized information* $(U, \psi p_i)$ corresponding to data $\psi_i = \psi p_i$ for some $1 \le i \le N$. Correspondingly, we obtain a finite element solution via:

$$\text{Compute } \hat{U}_i \in \hat{V}_i \text{ such that } A(\hat{U}_i, v) = (f, v) \text{ for all } v \in \hat{V}_i, \tag{5.4}$$

where $\hat{V}_i$ is a space of continuous, piecewise linear functions on a locally quasi-uniform simplex triangulation $\mathcal{T}_i$ of Ω obtained by (presumably local) refinement of an initial coarse triangulation $\mathcal{T}_0$ of Ω. We emphasize that the space $\{\hat{V}_i\}$ is globally defined and the "localized" problem (5.4) is solved over the entire domain, though we hope that (5.4) will require a locally refined mesh because the corresponding data has localized support.

We can obtain a partition of unity approximation in the sense of Babuška and Melenk [1] by defining the truly local approximations $U_i = \chi_i \hat{U}_i$, $1 \le i \le N$, where χ_i is the characteristic function of Ω_i. The local approximation U_i is in the local finite element space $V_i = \chi_i \hat{V}_i$. The *partition of unity approximation* is defined by $U_p = \sum_{i=1}^N U_i p_i$, which is in the *partition of unity finite element space*

$$V_p = \sum_{i=1}^N V_i p_i = \left\{ \sum_{i=1}^N v_i p_i : v_i \in V_i \right\}.$$

The basic convergence results for this method are proved in [17] and [18] using ideas of Babuška and Melenk [1] and Xu and Zhou [21]. The upshot is that the partition of unity approximation recovers the full convergence properties of an approximation of the original solution. Note that

$$U_p = \sum_{i=1}^N U_i p_i = \sum_{i=1}^N \chi_i \hat{U}_i p_i \equiv \sum_{i=1}^N \hat{U}_i p_i.$$

In words, the values of U_i or $\hat{U}_i$ outside of Ω_i are immaterial in forming the global partition of unity approximation.

To estimate the error in the localized information corresponding to ψ_i, we use the generalized Green's function satisfying the adjoint problem:

$$\text{Find } \phi_i \in H_0^1(\Omega) \text{ such that } A^*(v, \phi_i) = (v, \psi_i) \text{ for all } v \in H_0^1(\Omega). \qquad (5.5)$$

We expand the global error in the partition of unity approximation as

$$(u - U_p, \psi) = \sum_{i=1}^{N} \big((u - U_i)p_i, \psi\big).$$

We estimate each summand on the right as

$$\begin{aligned}
\big((u - U_i)p_i, \psi\big) &= (u - \hat{U}_i, \psi_i) = A^*(u - \hat{U}_i, \phi_i) \\
&= (f, \phi_i) - (a\nabla\hat{U}_i, \nabla\phi_i) - (b \cdot \nabla\hat{U}_i, \phi_i) - (c\hat{U}_i, \phi_i).
\end{aligned}$$

Letting $\pi_i\phi_i$ denote an approximation of ϕ_i in $\hat{V}_i$, using Galerkin orthogonality, we conclude

THEOREM 5.1. *The error of the partition of unity finite element solution U_p satisfies the error representation,*

$$\begin{aligned}
(u - U_p, \psi) = \sum_{i=1}^{N} \big((f, \phi_i - \pi_i\phi_i) - (a\nabla\hat{U}_i, \nabla(\phi_i - \pi_i\phi_i)) - (b \cdot \nabla\hat{U}_i, \phi_i - \pi_i\phi_i) \\
- (c\hat{U}_i, \phi_i - \pi_i\phi_i)\big), \quad (5.6)
\end{aligned}$$

where ϕ_i is the solution of the adjoint problem (5.5) and $\hat{U}_i$ solves the finite element problem (5.4) corresponding to the localized data ψ_i.

In practice, we compute approximate generalized Green's functions via;

$$\text{Compute } \Phi_i \in V_i^2 \text{ such that } A^*(v, \Phi_i) = (v, \psi_i) \text{ for all } v \in V_i^2, \quad 1 \leq i \leq N, \quad (5.7)$$

where V_i^2 is the space of continuous, piecewise quadratic functions with respect to $\mathcal{T}_i$. The corresponding approximate error representation for each computation is

$$\begin{aligned}
(u - \hat{U}_i, \psi_i) \approx (f, \Phi_i - \pi_i\Phi_i) - (a\nabla\hat{U}_i, \nabla(\Phi_i - \pi_i\Phi_i)) - (b \cdot \nabla\hat{U}_i, \Phi_i - \pi_i\Phi_i) \\
- (c\hat{U}_i, \Phi_i - \pi_i\Phi_i). \quad (5.8)
\end{aligned}$$

Note that the proof of Theorem 5.1 also implies that if the localized error satisfies

$$\big|(u - \hat{U}_i, \psi_i)\big| \leq \frac{\text{TOL}}{N}, \quad 1 \leq i \leq N, \qquad (5.9)$$

then $|(u - U_p, \psi)| \leq \text{TOL}$. This justifies treating the N "localized" problems independently in terms of mesh refinement. Note however that (5.9) is based on the pessimistic assumption that there is no cancellation of errors when combining the "localized" solutions to get the full solution. Using TOL/N for the tolerance for the "localized" solutions turns out to be much too pessimistic in practice. Finding more reasonable tolerances is an interesting problem.

6. Efficient computation of multiple quantities of interest using the effective domain of influence. In this section, we develop an algorithm for computing multiple quantities of interest efficiently using knowledge of the effective domains of influence of the corresponding Green's functions. We assume that the information is specified as $\{(U, \psi_i)\}_{i=1}^{N}$ for a set of N functions $\{\psi_i\}_{i=1}^{N}$. These data might arise as particular goals or via localization through a partition of unity. We assume that the goal is to compute the information associated to ψ_i so that the error is smaller than a tolerance TOL_i for $1 \leq i \leq N$.

At least two approaches for this problem come to mind:

Approach 1: **A Global Computation**
Find one triangulation such that the corresponding finite element solution satisfies $|(e, \psi_i)| \leq \mathrm{TOL}_i$, for $1 \leq i \leq N$.

Approach 2: **A Decomposed Computation**
Find N independent triangulations and finite element solutions U_i so that the errors satisfy $|(e_i, \psi_i)| \leq \mathrm{TOL}_i$, for $1 \leq i \leq N$.

Note that the Global Computation can be implemented with a straightforward modification of the standard adaptive strategy in which the N corresponding mesh acceptance criteria are checked on each element and if any of the N criteria fail, the element is marked for refinement.

Generally, if the correlation, i.e., overlap, between the effective domains of influence associated to the N data $\{\psi_i\}$ is relatively small and the effective domains of influence are relatively small subsets of Ω, then each individual solution in the Decomposed Computation will require significantly fewer elements than the solution in the Global Computation to achieve the desired accuracy. This can yield significant computational advantage in terms of lowering the maximum memory requirement to solve the problem. We provide some examples showing the possible gain in Sec. 8.

Decreasing the maximum memory required to solve a problem can be significant in at least two situations. First, if the individual solutions in the Decomposed Computation are computed in parallel, then the time needed for the Decomposed Computation is determined roughly by the time it takes to solve for the solution requiring the largest number of elements. If the individual solutions in the Decomposed Computation require significantly fewer elements than the Global Computation, we can expect to see significant speedup. Second, if we are solving in an environment with limited memory capabilities, then decomposing a Global Computation requiring a large number of elements into a set of significantly smaller computations can greatly increase the accuracy of the solution that can be computed and/or decrease the time of solution. In this case, the individual solutions in the Decomposed Computation may be computed serially.

Vice versa, if the effective domains of influence associated to the N data $\{\psi\}$ have relatively large intersections, then the individual solutions in the Decomposed Computation will require roughly the same number of elements as the solution for the Global Computation. In this case, there is little to be gained in using the Decomposed Computation. In general, we can expect that some of the N effective domains of influence associated to data $\{\psi_i\}$ in the Decomposed Computation will correlate significantly and the rest will have low correlation. We can optimize the use of resources by combining computations for data whose associated domains of influence have significant correlation and treating the rest independently.

An algorithm for the decomposition of the solution process using effective domains of influence is:

ALGORITHM 6.1. **Determining the Solution Decomposition**
1. *Discretize Ω by an initial coarse triangulation $\mathcal{T}_0$ and compute an initial finite element solution U_0.*
2. *Estimate the error in each quantity (U_0, ψ_i) by solving the N approximate adjoint problems (5.7) and then using (5.8).*
3. *Using the element indicators associated to (5.8) to identify the effective domains of influence for the data $\{\psi_i\}$ in terms of the mesh $\mathcal{T}_0$ and significant correlations between the effective domains of influence.*
4. *Decide on the number of approximate solutions to be computed and the subset of information to be computed from each solution.*
5. *Compute the approximate solutions independently using adaptive error control aimed at computing the specified quantity or quantities of interest accurately.*

We address the key step 3. in the practical implementation of this algorithm in Sec. 7.

7. Identifying significant correlations between effective domain of influences. The key issue in implementing Algorithm 6.1 is identifying the effective domains of influence for the various generalized Green's functions and recognizing significant correlation, or overlap, between different effective domains of influence in Step 3. In this section, we present a method to do this.

Recall from Sec. 4 that the mesh refinement decisions are based on the sizes of the element indicators on element K,

$$\mathcal{E}_i|_K = \max_K \left| (f - b \cdot \nabla \hat{U}_i - c\hat{U}_i)(\Phi_i - \pi_i \Phi_i) - a\nabla \hat{U}_i \cdot \nabla(\Phi_i - \pi_i \Phi_i) \right| \qquad (7.1)$$

or

$$\mathcal{E}_i|_K = \int_K \left| (f - b \cdot \nabla \hat{U}_i - c\hat{U}_i)(\Phi_i - \pi_i \Phi_i) - a\nabla \hat{U}_i \cdot \nabla(\Phi_i - \pi_i \Phi_i) \right| dx, \qquad (7.2)$$

associated to the estimate (5.8). We let $\mathcal{E}_i(x)$ denote the piecewise constant *element error indicator function* associated to data ψ_i with $\mathcal{E}_i(x) \equiv \mathcal{E}_i|_K$ for $K \in \mathcal{T}_0$.

Identifying the effective domain of influence associated to a data means finding a set of elements on which the element error indicators are significantly larger than on the complement, if such a dichotomy exists. Identifying significant correlation between the effective domains of influence of two data entails showing that the effective domains of influence have a significant number of elements in common.

To do this, we borrow techniques from pattern matching in signal processing. Of particular importance is the *(cross-)correlation* of two functions $f \in L^p(\Omega)$ and $g \in L^q(\Omega)$, defined as:

$$(f \circ g)(y) = \int_\Omega f(x)g(y + x)\, dx,$$

which is an $L^1(\Omega)$ function. In template matching algorithms used in image and signal processing, the correlations between an input signal and a library of signals are computed and the closest match from the library is the signal containing the "largest" correlation function in some measure. Since each correlation function is itself a real-valued function of n variables, determining the goodness of a match requires computing some real-valued *correlation indicator* $c(f, g)$ of the correlation function $(f \circ g)$, which is typically an L^p-norm.

For the problem of recognizing correlation between effective domains of influence, we treat the element error indicator functions $\{\mathcal{E}_i\}$ as signal functions. In this case, if one signal matches the other signal only after a translation or rotation, we do not consider the functions to be well correlated since this coincides with two primarily disjoint effective domains of influence. Without translation or rotation, correlation of $\mathcal{E}_i$ and $\mathcal{E}_j$ reduces to the L^2-inner-product:

$$(\mathcal{E}_i \circ \mathcal{E}_j)(0) = \int_\Omega \mathcal{E}_i(x)\mathcal{E}_j(x)\,dx = (\mathcal{E}_i, \mathcal{E}_j)_\Omega.$$

The correlation function evaluated at $u = 0$ is just a real number, so that the correlation indicator $c(\mathcal{E}_i, \mathcal{E}_j)$ can be taken as $c(\mathcal{E}_i, \mathcal{E}_j) = |(\mathcal{E}_i \circ \mathcal{E}_j)(0)| = (\mathcal{E}_i, \mathcal{E}_j)_\Omega$.

We mark the effective domain of influence associated to ψ_i as significantly correlated to the domain of influence associated to ψ_j if two conditions hold:

1. The correlation of $\mathcal{E}_i$ and $\mathcal{E}_j$ is larger than a fixed fraction of the norm of $\mathcal{E}_j$, or mathematically,

$$\text{Correlation Ratio 1} = \frac{c(\mathcal{E}_i, \mathcal{E}_j)}{\|\mathcal{E}_j\|^2} \geq \gamma_1, \tag{7.3}$$

   for some fixed $0 \leq \gamma_1 \leq 1$. This means that the projection of $\mathcal{E}_i$ onto $\mathcal{E}_j$ is sufficiently large.

2. The component of $\mathcal{E}_j$ orthogonal to $\mathcal{E}_i$ is smaller than a fixed fraction of the norm of $\mathcal{E}_j$, or mathematically,

$$\text{Correlation Ratio 2} = \frac{\left\| \mathcal{E}_j - \dfrac{c(\mathcal{E}_j, \mathcal{E}_i)}{\|\mathcal{E}_i\|^2} \mathcal{E}_i \right\|}{\|\mathcal{E}_j\|} \leq \gamma_2, \tag{7.4}$$

   for some fixed $0 \leq \gamma_2 \leq 1$. This corrects for the potential difficulties in the mesh refinement decision that arise when $\mathcal{E}_i$ is much larger than $\mathcal{E}_j$ and the corresponding computations are combined.

In general, both Correlation Ratios converge to a limit as the number of elements increases. Moreover, the second Correlation Ratio varies relatively little as the mesh density changes for all kinds of data. The first Correlation Ratio for data representing a partition of unity decomposition also varies relatively little as the mesh density changes. However, the first Correlation Ratio varies quite a bit on coarse meshes when one of the data is an approximate delta function. We find that the determination that two effective domains of influence are *not* closely correlated seems to be relatively invariant with respect to the density of the mesh. However, the determination that two effective domains of influence are correlated does vary with mesh density and there is a mild tendency to combine computations that are more efficiently treated independently if the correlation indicators are computed on very coarse meshes.

We emphasize that the initial identification of significant correlation between effective domains of influence of various Green's functions in a computation is carried out on a coarse initial partition of the domain and hence is relatively inexpensive.

8. Computational examples. In this section, we present several computational examples illustrating and testing the ideas in this paper. In these experiments, we solve various elliptic problems using adaptive mesh refinement to achieve a specified accuracy in a specified set of quantities of interest first using a Global Computation and then using a Decomposed Computation implemented using Algorithm 6.1. The

results suggest that the individual solutions in the Decomposed Computation require significantly fewer elements to achieve the desired accuracy than the Global Computation in a variety of situations.

Determining the overall gain in efficiency or capability due to reducing the number of elements to achieve a desired accuracy is difficult. In general, the principle factors determining the time it takes for a solution to be computed, including the solution of the nonlinear system determining the approximation, the marking and refinement of meshes in each refinement level, and, in a massively parallel setting, the IO of the data, all scale super-linearly with the number of elements. Moreover, these factors depend heavily on the algorithm, implementation, and machine. So, as a relatively universal measure of the gain from using the Decomposed Computation, we report the *Final Element Ratio* of the number of elements in the final mesh refinement level required to achieve the specified accuracy in the specified quantities of interest in the Global Computation to the **maximum** number of elements in the final mesh refinement levels for the individual computations in the Decomposed Computation. Generally, we expect the gain in efficiency to scale super-linearly with the Final Element Ratio.

All computations are performed using *FETkLab* [11]. This adaptive finite element code, running under *MATLAB*, can solve general nonlinear elliptic systems on general domains in two space dimensions. It implements the *a posteriori* error estimate described in Sec. 4, allowing up to 16 simultaneous adjoint data ψ_i to be specified. In the computations below, we use red-green quadrisection to refine elements, where the elements marked for refinement are refined using quadrisection while the resulting nonconforming border elements are fixed using bisection. To reduce over-refinement in any one level, only those elements whose element indicators are larger than the mean plus one standard deviation of all of the element indicators in that level are refined.

8.1. Example 1. We test the partition of unity decomposition of a solution aimed at computing information corresponding to data with global support. We approximate u satisfying the Poisson problem with smooth data,

$$\begin{cases} -\frac{1}{10\pi^2}\Delta u(x) = \sin(\pi x)\sin(\pi y), & (x,y) \in \Omega, \\ u(x,y) = 0, & (x,y) \in \partial\Omega, \end{cases} \tag{8.1}$$

on the domain $\Omega = [0,8] \times [0,8]$. The solution is $u(x,y) = 5\sin(\pi x)\sin(\pi y)$. We solve this problem with the goal of controlling the error in the average value of u by choosing $\psi \equiv 1/|\Omega| = 1/64$.

For the Global Computation, we use a tolerance of 5% for the error in the average. We begin with an initial mesh of 10×10 elements. After five refinement levels, we end up with 3505 elements, achieving an error of .022. We plot both the initial and final meshes in Fig. 8.1. We plot the numerical solution on the final mesh in Fig. 8.2.

Since we know the true solution, we can compute the actual average error and so evaluate the accuracy of the estimate. Below, we list the estimates, errors, and error/estimate ratios:

Level	Elts.	Estimate	Error	Ratio	Level	Elts.	Estimate	Error	Ratio
1	100	.1567	.1534	.9786	4	1309	.1159	.1166	1.006
2	211	.1157	.1224	1.058	5	3505	.02163	.02148	.9975
3	585	.3063	.3078	1.005					

We see the excellent accuracy of the computed error estimate at all levels of mesh refinement, which is typical with this approach to *a posteriori* error estimation.
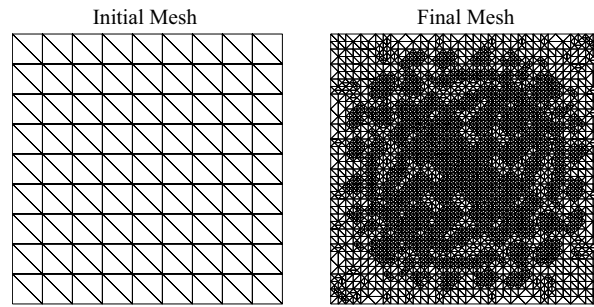
Initial Mesh   Final Mesh

FIG. 8.1. *Initial and final meshes for Example 1 with data ψ giving the average error.*
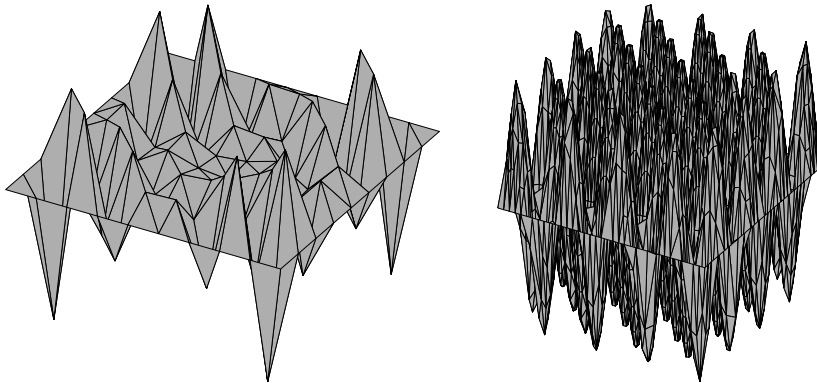

FIG. 8.2. *Numerical solutions on the initial (left) and final (right) meshes for Example 1 with data ψ giving the average error.*

Note, that in this example, we can also estimate the L^2 error using $\psi = e/\|e\|_\Omega$. The results are similarly satisfying. In the examples following, we do not have a true solution available, so we continue to use the error in the average for the sake of consistency.

The data $\psi \equiv 1/64$ is a natural candidate for localization using a partition of unity. We begin with a partition with the four domains shown on the left in Fig. 8.3. Introducing the corresponding partition of unity yields four data $\{\psi_1, \psi_2, \psi_3, \psi_4\}$ cor-
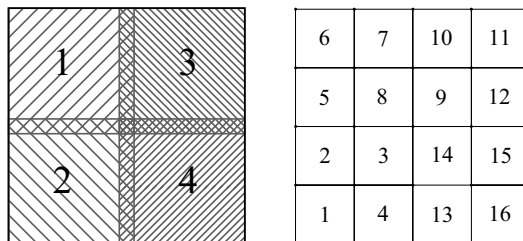

6	7	10	11
5	8	9	12
2	3	14	15
1	4	13	16

FIG. 8.3. *Domains for the first (left) and second (right) partitions of unity used in Example 1.*

responding to the regions indicated in Fig. 8.3.

In the first Decomposed Computation, we compute the four localized approximations $\{\hat{U}_1, \cdots, \hat{U}_4\}$ using the same initial mesh as shown in Fig. 8.1. Using $\gamma_1 = .9$

and $\gamma_2 = .5$ in the conditions on the Correlation Ratios (7.3) and (7.4) indicates that all four localized solutions should be computed independently.

For the first Decomposed Computation, we obtain acceptable results using the tolerance of 5%. Details of the final computed solutions are listed below:

Data	Level	Elements	Estimate
ψ_1	3	618	.01242
ψ_2	3	575	$-.0009109$
ψ_3	3	618	.01242
ψ_4	3	575	$-.0009109$

Combining these solutions yields a partition of unity solution U_p with accuracy .023. Using the Decomposed Computation yields a Final Element Ratio of $3505/618 \approx 5.7$.

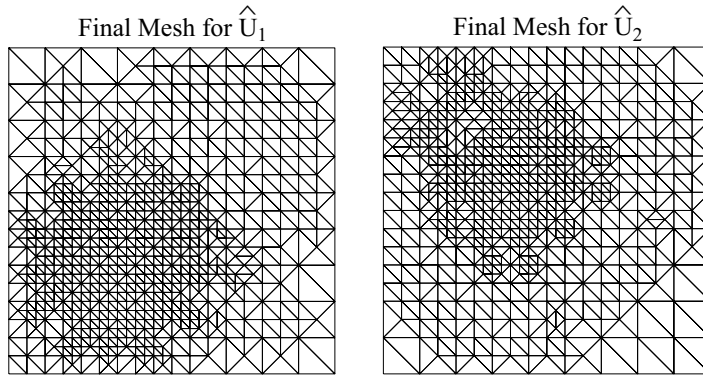We plot the final meshes for two of the computations in Fig. 8.4. We plot the

Final Mesh for $\widehat{U}_1$ Final Mesh for $\widehat{U}_2$

FIG. 8.4. *Final meshes for $\hat{U}_1$ and $\hat{U}_2$ for Example 1 with a partition of unity on four domains.*

generalized Green's functions for the global average error and the localized solution corresponding to ψ_2 in Fig. 8.5. The decay of influence away from the support of ψ_2 is clearly visible in the solution on the right.
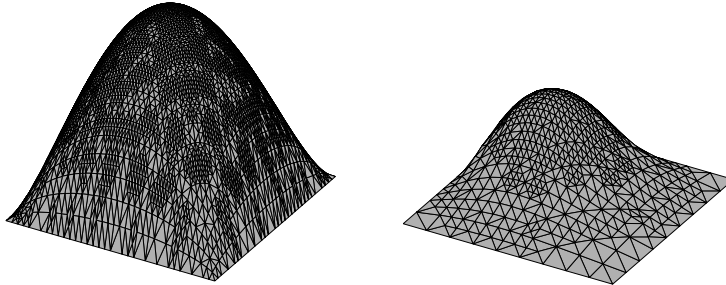

FIG. 8.5. *The generalized Green's functions for the global average error and the localized solution $\hat{U}_2$ corresponding to ψ_2 with a partition of unity on four domains.*

Next, we perform a Decomposed Computation using a partition of unity on the 16 equal-sized regions shown on the right in Fig. 8.3. We again use an error tolerance of 5% and start the localized computations with the same initial 10×10 mesh used above. Computing the correlation ratios, we find these significant correlations:

$\mathcal{E}_2$ with $\mathcal{E}_3$ $\mathcal{E}_5$ with $\mathcal{E}_8$ $\mathcal{E}_{10}$ with $\mathcal{E}_9$ $\mathcal{E}_{13}$ with $\mathcal{E}_{14}$
$\mathcal{E}_4$ with $\mathcal{E}_3$ $\mathcal{E}_7$ with $\mathcal{E}_8$ $\mathcal{E}_{12}$ with $\mathcal{E}_9$ $\mathcal{E}_{15}$ with $\mathcal{E}_{14}$

This suggests that we should see less gain on this partition. In order to obtain an acceptable accuracy in the four sub-domains closest to the center, we have to use an extra refinement level in the computation of the corresponding local solutions. The error in the average of the resulting partition of unity solution is .011. If we use the Decomposed Computation, the most intensive individual computations are those for ψ_3 and ψ_9, which yields a Final Element Ratio of $3505/1371 \approx 2.6$. There is still a significant gain over the Global Computation, but not as large as for the partition with four sub-domains.

8.2. Example 2. We estimate the error in some point values and the average value of u solving

$$
\begin{cases}
-\nabla \cdot \big((1.1 + \sin(\pi x)\sin(\pi y))\nabla u(x,y)\big) \\
\quad = -3\cos^2(\pi x) + 4\cos^2(\pi x)\cos^2(\pi x) \\
\quad\quad +2.2\sin(\pi x)\sin(\pi y) + 2 - 3\cos^2(\pi y), \quad (x,y) \in \Omega, \\
u(x,y) = 0, \hspace{6.5cm} (x,y) \in \partial\Omega,
\end{cases}
\tag{8.2}
$$

where $\Omega = [0,2] \times [0,2]$ and the exact solution is $u(x,y) = \sin(\pi x)\sin(\pi y)$. We compute the average error corresponding to $\psi_1 \equiv 1/4$ and then four point values corresponding to $\psi_2 \approx \delta_{(.5,.5)}$, $\psi_3 \approx \delta_{(.5,1.5)}$, $\psi_4 \approx \delta_{(1.5,1.5)}$, and $\psi_5 \approx \delta_{(1.5,.5)}$. We use

$$
\hat{\delta}_{(c_x,c_y)} = \frac{400}{\pi} e^{-400((x-c_x)^2 + (y-c_y)^2)}
$$

to approximate the delta function $\delta_{(c_x,c_y)}$.

In the Global Computation, we compute a mesh that gives all of the desired information accurately using a tolerance of 2%. We begin with an 8×8 mesh. We list the results below:

Lev.	Elt's	ψ_1			ψ_2 and ψ_4			ψ_3 and ψ_5		
		Est.	Err.	Rat.	Est.	Err.	Rat.	Est.	Err.	Rat.
1	64	.035	.035	1.0	.090	.29	3.3	.24	.022	.091
2	201	.0088	.0089	1.0	.042	.082	1.9	.0024	.014	6.0
3	763	.0027	.0027	1.0	.020	.020	.99	.0020	.0020	1.0
4	2917	.00044	.00044	1.0	.0050	.00504	1.0	.0049	.00504	1.0

We obtain an acceptably accurate solution after four refinement levels using a mesh with 2917 elements. Note that the estimates for the point values become very accurate on mesh of moderate density and finer, which place sufficient elements near the center of the corresponding delta functions.

We next perform a Decomposed Computation by solving for approximate solutions $\{\hat{U}_1, \cdots, \hat{U}_5\}$ corresponding to each data $\{\psi_1, \cdots, \psi_5\}$ independently. Checking the Correlation Ratios reveals no significant correlations between the independent error indicators. To obtain final independent solutions that yield roughly the same accuracy in the computed quantities as the solution of the Global Computation, we use a tolerance of 2% and uniform initial meshes that are 7×7 for $\hat{U}_1$; 9×9 for $\hat{U}_2$ and $\hat{U}_4$; and 12×12 for $\hat{U}_3$ and $\hat{U}_5$. The final results for each computation are listed below:

Data	Level	Elements	Estimate
ψ_1	3	409	$-.0004699$
ψ_2	4	1037	$-.007870$
ψ_3	2	281	$-.005571$
ψ_4	4	1037	$-.007870$
ψ_5	2	281	$-.005571$

The Final Element Ratio is $2917/1037 \approx 2.8$.

8.3. Example 3. We consider a problem with diffusion that is nearly singular at one point and that has strong convection, for which there is no precise analytic information about the generalized Green's function. We estimate the error in the average value of u solving

$$\begin{cases} -\nabla \cdot \left(\left(.05 + \tanh\left(10(x-5)^2 + 10(y-1)^2\right)\right)\nabla u\right) \\ \qquad\qquad\qquad + \begin{pmatrix} -100 \\ 0 \end{pmatrix} \cdot \nabla u = 1, \quad (x,y) \in \Omega, \\ u(x,y) = 0, \qquad\qquad\qquad\qquad\qquad\qquad\quad (x,y) \in \partial\Omega, \end{cases} \quad (8.3)$$

where $\Omega = [0,10] \times [0,2]$. The diffusion is 1 over most of Ω, but drops to .05 near $(5,1)$. Because of the sign of the convection, we expect that perturbations to the solution at a point with x-coordinate x_0 will affect the solution's values "downstream" for $x < x_0$ most strongly. The Peclet number for this problem is $Pe = 1000$.

We begin the computations with an initial mesh of 80 elements. For the Global Computation, we use an error tolerance of $TOL = .04\%$. We list some details of the computation below:

Level	Elements	Estimate	Level	Elements	Estimate
1	80	$-.0005919$	5	1809	$-.0001070$
2	193	$-.001595$	6	3849	$-.00004073$
3	394	$-.0009039$	7	9380	$-.00001715$
4	828	$-.0003820$	8	23989	$-.000007553$

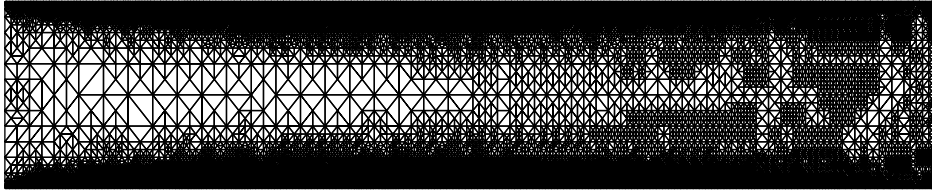We plot the final mesh in Fig. 8.6. The effects of the convection are clear in the

FIG. 8.6. *Plot of the final mesh for Example 3 with data ψ giving the average error.*

pattern of mesh refinement.

Next, we consider the partition of unity with 20 subdomains shown in Fig. 8.7. Computing the Correlation Ratios, we find the significant correlations:

11	12	13	14	15	16	17	18	19	20
1	2	3	4	5	6	7	8	9	10

FIG. 8.7. *Domains for the partition of unity used in Example 3.*

$\mathcal{E}_3$ with $\mathcal{E}_4$ $\quad\quad$ $\mathcal{E}_6$ with $\mathcal{E}_7$ $\quad\quad$ $\mathcal{E}_7$ with $\mathcal{E}_6$ $\quad\quad$ $\mathcal{E}_9$ with $\mathcal{E}_8$ $\quad\quad$ $\mathcal{E}_{10}$ with $\mathcal{E}_8, \mathcal{E}_9$
$\mathcal{E}_{13}$ with $\mathcal{E}_{14}$ $\quad$ $\mathcal{E}_{16}$ with $\mathcal{E}_{17}$ $\quad$ $\mathcal{E}_{17}$ with $\mathcal{E}_{16}$ $\quad$ $\mathcal{E}_{19}$ with $\mathcal{E}_{18}$ $\quad$ $\mathcal{E}_{20}$ with $\mathcal{E}_{18}, \mathcal{E}_{19}$

We compute the localized solutions $\{\hat{U}_i\}$ in the Decomposed Computation using two tolerances. Details of the final computed solutions are listed below. The results are

completely symmetric across $y = 1$.

Data	TOL	Lev.	Elts.	Est. $\times 10^{-7}$	Data	TOL	Lev.	Elts.	Est. $\times 10^{-7}$
ψ_1	.04%	7	7334	-6.927	ψ_6	.02%	7	6613	-2.471
ψ_2	.04%	7	8409	-5.986	ψ_7	.02%	7	4396	-2.938
ψ_3	.04%	7	7839	-5.189	ψ_8	.02%	7	4248	-1.656
ψ_4	.04%	7	7177	-5.306	ψ_9	.02%	7	3506	-1.221
ψ_5	.04%	7	7301	-4.008	ψ_{10}	.02%	7	1963	$-.5550$

The estimate on the total average error of U_p is 7.24×10^{-6} and the Final Element Ratio is $23909/8409 \approx 2.9$.

    We show a sample of the final meshes for the Decomposed Computation in Fig. 8.8. The effect of the convection is clearly visible in the pattern of mesh refinement. We
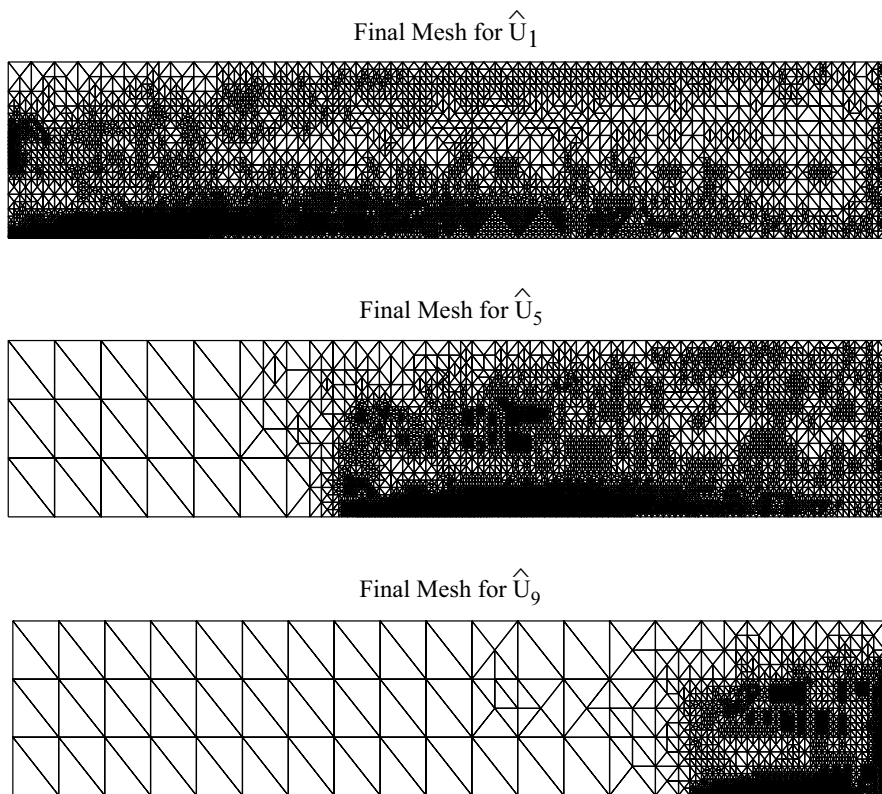
Final Mesh for $\widehat{U}_1$

Final Mesh for $\widehat{U}_5$

Final Mesh for $\widehat{U}_9$

FIG. 8.8. *Plots of the final meshes for the localized solutions $\hat{U}_1$, $\hat{U}_5$, and $\hat{U}_9$ in Example 3.*

can also see this in the graphs of the generalized Green's functions. We plot a sample in Fig. 8.9. In general, effective domains of influence may not be spatially compactly-shaped. The upper plot in Fig. 8.8 shows this situation. The effective domain of influence for the average value of the solution in the lower left corner of the domain, close to the "outflow" boundary at $x = 0$, contains the immediate neighborhood of the boundary along $y = 0$, a swath that cuts up from the center of the "outflow" boundary through the center of the domain up to the upper boundary, and most of the "inflow" boundary.

    Given the significant correlations listed above, we combine some of the localized computations by solving for localized solutions corresponding to summing the two of
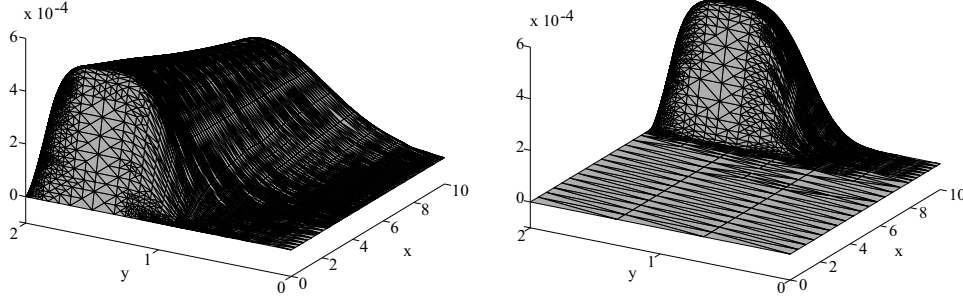
FIG. 8.9. *Plots of the generalized Green's functions corresponding to ψ_{11} (left) and ψ_{19} (right) in Example 3.*

the partition of unity data. We list details of the final computed solutions below:

Data	TOL	Level	Elements	Est. $\times 10^{-7}$
$\psi_3 + \psi_4$	.04%	7	8330	-9.8884
$\psi_6 + \psi_7$	.02%	7	5951	-5.897
$\psi_8 + \psi_9$	.02%	7	4406	-3.486
$\psi_9 + \psi_{10}$	.02%	7	3202	-2.243

The solutions for $\psi_3 + \psi_4$ and $\psi_8 + \psi_9$ use a few more elements than required for either of the original localized solutions. The solutions for $\psi_6 + \psi_7$ and $\psi_9 + \psi_{10}$ use less than the maximum required for the individual localized solutions.

8.4. Example 4. We consider a problem posed on a more complicated domain. We estimate the error in the average value of u solving

$$\begin{cases} -\frac{1}{\pi^2}\Delta u = 2 + 4e^{-5((x-.5)^2 + (y-2.5)^2)}, & (x,y) \in \Omega, \\ u(x,y) = 0, & (x,y) \in \partial\Omega, \end{cases} \tag{8.4}$$

where Ω is the "square annulus" $\Omega = [0,3] \times [0,3] \setminus [1,2] \times [1,2]$ shown in Fig. 8.12.

We begin the computations with an initial mesh of 48 elements. For the Global Computation, we use an error tolerance of $TOL = 1\%$. We list some details of the computation below:

Level	Elements	Estimate	Level	Elements	Estimate
1	48	-5.168	4	894	$-.3029$
2	125	-1.584	5	2075	$-.1435$
3	380	$-.6879$			

We plot the initial and final meshes in Fig. 8.10. Note the expected refinement required near the interior corners. We plot the final solution and generalized Green's function in Fig. 8.11.

Next, we consider the partition of unity with 8 subdomains shown in Fig. 8.12. Checking the Correlation Ratios reveals no significant correlations. We obtain acceptable results in the Decomposed Computation using the tolerance of 1%. Details of the final computed solutions are listed below:

Data	Level	Elements	Estimate	Data	Level	Elements	Estimate
ψ_1	5	1082	$-.01935$	ψ_5	5	1104	$-.01436$
ψ_2	5	1101	$-.01399$	ψ_6	5	1110	$-.01587$
ψ_3	5	1144	$-.01540$	ψ_7	5	1074	$-.02529$
ψ_4	5	1107	$-.01360$	ψ_8	5	1098	$-.01660$

Combining these solutions yields a partition of unity solution U_p with accuracy $-.1344$. Using the Decomposed Computation yields a Final Element Ratio of ≈ 1.8.
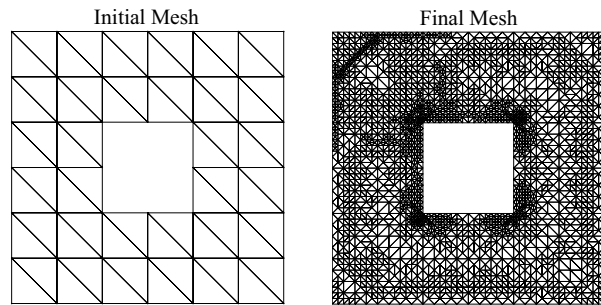
Initial Mesh   Final Mesh

FIG. 8.10. *Plots of the initial (left) and final (right) meshes for Example 4 with data ψ giving the average error.*
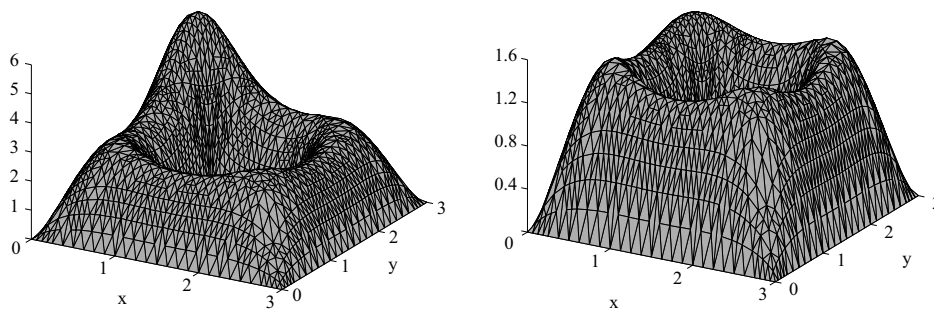

FIG. 8.11. *Plots of the final solution (left) and generalized Green's function (right) for Example 4 with data ψ giving the average error.*

We show a sample of the final meshes in Fig. 8.13 and a couple of the final generalized Green's functions in Fig. 8.14.

We also tried a partition of unity on a finer decomposition of Ω obtained by dividing each sub-domain in the first partition into four equal squares. However, the Final Element Ratio is only 1.09.

9. Conclusion. The *a posteriori* error analysis used in this paper takes into account the behavior of the generalized Green's function associated to the quantity of interest to determine the global effects of stability. The cost of this approach can be considerable, as it involves numerically solving the adjoint problem. One payoff is accuracy of the estimate.

We have demonstrated that, in certain situations, consideration of the approximate generalized Green's function can be used to improve the efficiency of the solution process. This possibility arises when the goal is to compute multiple quantities of interest and/or to compute quantities of interest that involve globally-supported information of the solution. In the latter case, we introduce a decomposition of solution that localizes the global computation by replacing it by a set of problems involving localized information. The decomposition allows recovery of the desired information by combining the local solutions. By treating each computation of a quantity of interest as an independent computation, we can reduce the maximum number of elements required to achieve a specified accuracy in the specified quantities of interest. This in turn can lead to significant computational gains in the settings of coarse-grained parallelization and memory-constrained computing environments.

7	6	5
8		4
1	2	3

FIG. 8.12. *Domains for the partition of unity used in Example 4.*

Final Mesh for $\hat{U}_6$ Final Mesh for $\hat{U}_7$
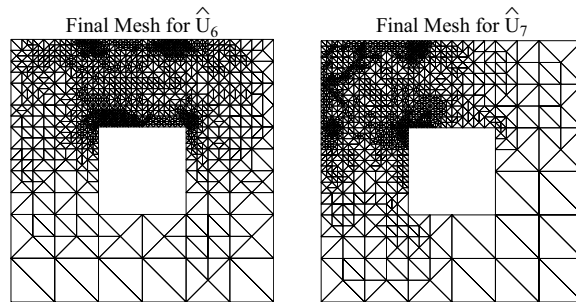
FIG. 8.13. *Plots of the final meshes for the localized solutions $\hat{U}_6$ and $\hat{U}_7$ in Example 4.*

We have demonstrated that significant gains are possible in a variety of situations using one analytic example and a series of computations. Moreover, the nature of elliptic problems means that we can expect even larger reduction on problems posed on three dimensional domains or complicated and large domains.

It is instructive to compare this decomposition of the solution with more traditional domain decomposition, which is a decomposition of the spatial domain. The spatial domain is partitioned into compactly-shaped sub-domains on which approximate problems that are completely local to the sub-domains are solved. Because the solution of the global problem generally involves transmission of information across the entire domain, approximating the global solution by local decomposition solutions involves iterations consisting of alternately passing information, e.g., through boundary conditions, between the sub-domains coupled with solving the localized problems. In contrast, we propose a decomposition of the solution operator associated to the differential equation, not of the domain. In traditional domain decomposition, any computational savings comes from solving problems that are truly localized. In the proposed approach, any savings comes from the use of coarse discretizations in a major part of the domain. It is important to note that effective domains of influence need not be compactly-shaped, as in Example 3 in Sec. 8.

This work suggests a new approach to traditional domain decomposition in which effective domains of influence are used instead of the traditional type of sub-domains. We conjecture that relatively few iterations would be required to obtain an accurate solution of the entire problem because of the reduced amount of information that would need to be passed between sub-domains consisting of different domains of influence.

Appendix. *Proof.* Following [9], to prove the *a posteriori* bound in Theorem 3.1, we break up the second integral on the right of (3.2) and use Green's formula on
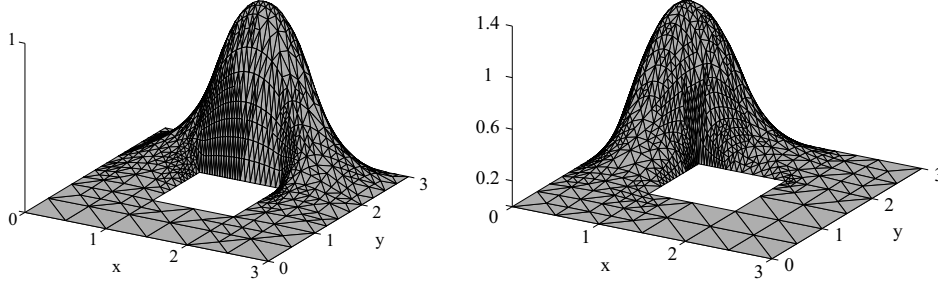
FIG. 8.14. *Plots of the generalized Green's functions corresponding to ψ_6 (left) and ψ_7 (right) for the partition of unity decomposition for Example 4.*

each element K to get

$$\int_\Omega \nabla U \cdot \nabla(\phi - \pi_h \phi)\,dx = \sum_{K \in \mathcal{T}_h} -\int_K \Delta U(\phi - \pi_h \phi)\,dx + \int_{\partial K} \nabla U \cdot n_{\partial K}(\phi - \pi_h \phi)\,ds.$$

Upon summing over all elements $K \in \mathcal{T}_h$, the boundary integrals give two contributions from each element edge, computed in opposite directions. The contribution from a common edge $\sigma_1 \subset \partial K_1 = \sigma_2 \subset \partial K_2$, where $K_1, K_2 \in \mathcal{T}_h$, is

$$\int_{\sigma_1} \nabla U|_{K_1} \cdot n_{\sigma_1}(\phi - \pi_h \phi)\,ds + \int_{\sigma_2} \nabla U|_{K_2} \cdot n_{\sigma_2}(\phi - \pi_h \phi)\,ds$$

$$= -\int_{\sigma_1} [\nabla U] \cdot n_{\sigma_1}(\phi - \pi_h \phi)\,ds.$$

When summing over the elements, we associate half of the common contribution across a shared edge between two elements with each element and obtain an alternate error representation,

$$\|e\|_{1,\omega} = -\sum_{K \in \mathcal{T}_h} \left(\int_K (\Delta U + f)(\phi - \pi_h \phi)\,dx - \frac{1}{2}\int_{\partial K} [\nabla U] \cdot n_{\partial K}(\phi - \pi_h \phi)\,ds \right).$$

The *a posteriori* bound follows upon taking norms and estimating.

The bound (3.3) on the first component of $\mathcal{R}_K$ is simple, $\|\Delta U + f\|_K = \|f\|_K \leq \max_\Omega |f| \times |K|^{1/2}$. To bound the second component, consider an integral over the common edge σ between two elements K_1 and K_2,

$$\|[\nabla U]\|_\sigma = \|\nabla U|_{K_2} - \nabla U|_{K_1}\|_\sigma \leq \|\nabla U|_{K_2} - \nabla u|_\sigma\|_\sigma + \|\nabla u|_\sigma - \nabla U|_{K_1}\|_\sigma.$$

By a trace inequality, the standard energy norm convergence result, and a standard elliptic regularity result, we have

$$\|\nabla U|_{K_i} - \nabla u|_\sigma\|_\sigma \leq \|\nabla U - \nabla u\|_{K_i}^{1/2}\|\nabla U - \nabla u\|_{1,K_i}^{1/2} \leq C\|hu\|_{2,K_i}^{1/2}\|u\|_{2,K_i}^{1/2}$$

$$\leq C\|h^{1/2}f\|_{K_i},$$

for $i = 1, 2$. The local quasi-uniformity of the mesh implies $\frac{1}{2}\|h^{-1/2}[\nabla U]\|_{\partial K} \leq C \max_\Omega |f| \times |K|^{1/2}$. $\square$

REFERENCES

[1] I. Babuška and J. Melenk, *The partition of unity finite element method*, Internat. J. Numer. Methods Engrg., 40 (1997), pp. 727–758.

[2] W. Bangerth and R. Rannacher, *Adaptive Finite Element Methods for Differential Equations*, Birkhauser, Boston, 2003.

[3] R. Bank and M. Holst, *A new paradigm for parallel adaptive mesh refinement*, SIAM J. Sci. Comput., 22 (2000), pp. 1411–1443.

[4] R. Becker and R. Rannacher, *An optimal control approach to a posteriori error estimation in finite element methods*, Acta Numerica, (2001), pp. 1–102.

[5] S. Brenner and L. R. Scott, *The Mathematical Theory of Finite Element Methods*, Springer-Verlag, New York, 1994.

[6] L. Dieci and D. Estep, *Some stability aspects of schemes for the adaptive integration of stiff initial value problems*, SIAM J. Sci. Stat. Comput., 12 (1991), pp. 1284–1303.

[7] K. Eriksson, D. Estep, P. Hansbo, and C. Johnson, *Introduction to adaptive methods for differential equations*, Acta Numerica, (1995), pp. 105–158.

[8] ———, *Computational Differential Equations*, Cambridge University Press, New York, 1996.

[9] K. Eriksson and C. Johnson, *Adaptive finite element methods for parabolic problems I: A linear model problem*, SIAM J. Numer. Anal., 28 (1991), pp. 43–77.

[10] D. Estep, *A posteriori error bounds and global error control for approximations of ordinary differential equations*, SIAM J. Numer. Anal., 32 (1995), pp. 1–48.

[11] D. Estep and M. Holst, *FETkLab: Finite Element Toolkit for MATLAB*, 2002. can be obtained from http://www.fetk.org.

[12] D. Estep, M. Holst, and D. Mikulencak, *Accounting for stability: a posteriori error estimates based on residuals and variational analysis*, Comm. Num. Meth. Engin., 18 (2002), pp. 15–30.

[13] D. Estep and R. Williams, *Accurate parallel integration of large sparse systems of differential equations*, Math. Models Meth. Appl. Sci., 6 (1996), pp. 535–568.

[14] D. J. Estep, M. G. Larson, and R. D. Williams, *Estimating the error of numerical solutions of systems of reaction-diffusion equations*, Memoirs A.M.S., 146 (2000), pp. 1–109.

[15] M. Giles and E. Süli, *Adjoint methods for pdes: a posteriori error analysis and postprocessing by duality*, Acta Numerica, (2002), pp. 145–236.

[16] M. Griebel and M. Schweitzer, *A particle-partition of unity method for the solution of elliptic, parabolic, hyperbolic pdes*, SIAM J. Sci. Comput., 22 (2000), pp. 853–890.

[17] M. Holst, *Adaptive numerical treatment of elliptic systems on manifolds*, Adv. Comput. Math., 15 (2001), pp. 139–191.

[18] ———, *Applications of domain decomposition and partition of unity methods in physics and geometry (plenary paper)*, in Fourteenth International Conference on Domain Decomposition Methods, January 2002, Mexico City, Mexico, 2002.

[19] C. Johnson, S. Larsson, V. Thomée, and L. Wahlbin, *Error estimates for spatially discrete approximations of semilinear parabolic equations with nonsmooth initial data*, Math. Comput., 49 (1987), pp. 331–357.

[20] J. Lions and E. Magenes, *Non-Homogeneous Boundary Value Problems and Applications*, vol. 1, Springer-Verlag, New York, 1972.

[21] J. Xu and A. Zhou, *Local and parallel finite element algorithms based on two-grid discretizations*, Math. Comput., 69 (2000), pp. 881–909.